


# Protein–nucleotide contacts in motor proteins detected by DNP-enhanced solid-state NMR

## Journal Article

### Author(s):

Wiegand, Thomas; Liao, Wei-Chih; Ong, Ta-Chung; Däpp, Alexander; Cadalbert, Riccardo; Copéret, Christophe ; Böckmann, Anja; Meier, Beat H.

### Publication date:

2017-11

### Permanent link:

<https://doi.org/10.3929/ethz-b-000211916>

### Rights / license:

[In Copyright - Non-Commercial Use Permitted](#)

### Originally published in:

Journal of Biomolecular NMR 69(3), <https://doi.org/10.1007/s10858-017-0144-3>

### Funding acknowledgement:

159707 - NMR studies in the Solid State (SNF)

146757 - NMR studies in the Solid State (SNF)

# Protein-nucleotide contacts in motor proteins detected by DNP-enhanced solid-state NMR

Thomas Wiegand<sup>a</sup>, Wei-Chih Liao<sup>b</sup>, Ta Chung Ong<sup>b</sup>, Alexander Däpp<sup>a</sup>,  
Riccardo Cadalbert<sup>a</sup>, Christophe Copéret<sup>b,\*</sup>, Anja Böckmann<sup>c,\*</sup> and Beat H.  
Meier<sup>a,\*</sup>

<sup>a</sup>*Physical Chemistry, ETH Zurich, 8093 Zurich, Switzerland*

<sup>b</sup>*Department of Chemistry and Applied Biosciences – Inorganic Chemistry, ETH Zurich, 8093 Zurich, Switzerland*

<sup>c</sup>*Institut de Biologie et Chimie des Protéines, Bases Moléculaires et Structurales des Systèmes Infectieux, Labex Ecofect, UMR 5086 CNRS, Université de Lyon, 7 passage du Vercors, 69367 Lyon, France*

\*Corresponding authors: [ccoperet@ethz.ch](mailto:ccoperet@ethz.ch), [a.boeckmann@ibcp.fr](mailto:a.boeckmann@ibcp.fr), [beme@ethz.ch](mailto:beme@ethz.ch)

## **Abstract**

DNP (dynamic nuclear polarization)-enhanced solid-state NMR is employed to directly detect protein-DNA and protein-ATP interactions and identify the residue type establishing the intermolecular contacts. While conventional solid-state NMR can detect protein-DNA interactions in large oligomeric protein assemblies in favorable cases, it typically suffers from low signal-to-noise ratios. We show here, for the oligomeric DnaB helicase from *Helicobacter pylori* complexed with ADP and single-stranded DNA, that this limitation can be overcome by using DNP-enhanced spectroscopy. Interactions are established by DNP-enhanced  $^{31}\text{P}$ - $^{13}\text{C}$  polarization-transfer experiments followed by the recording of a 2D  $^{13}\text{C}$ - $^{13}\text{C}$  correlation experiment. The NMR spectra were obtained in less than two days and allowed the identification of residues of the motor protein involved in nucleotide binding.

## Introduction

The direct observation of protein-nucleotide interactions in NMR requires the observation of dipolar correlations between spins on both the nucleotide and the protein. In solution-state NMR, homonuclear and heteronuclear NOE contacts can be exploited (e.g.  $^1\text{H}$ - $^1\text{H}$  NOE contacts combined with  $^{13}\text{C}/^{15}\text{N}$  editing or filtering), while in solid-state NMR dipolar-mediated polarization transfer is the method of choice<sup>1-3</sup>. In particular,  $^{31}\text{P}$ (nucleotide)- $^{13}\text{C}$ (protein) transfer does not only benefit from the high gyromagnetic ratio of  $^{31}\text{P}$ , but is also at the core of understanding protein–nucleotide interactions. For instance, Goldbourn and coworkers have studied a capsid of the fd bacteriophage with a 50-residue major coat protein by  $^{31}\text{P}$ - $^{13}\text{C}$  polarization transfer via protons<sup>4</sup> (termed PHHC in analogy to CHHC experiments used in protein structure calculation<sup>5</sup>) to determine capsid-DNA interactions. However, such experiments often suffer from low signal-to-noise ratios in particular for large protein complexes.

Dynamic nuclear polarization (DNP)-based techniques can significantly enhance the signal-to-noise ratio of NMR<sup>6,7</sup> and have been applied to the structural elucidation of biological systems, for a recent review see reference<sup>8</sup>. A general drawback of biomolecular MAS-DNP studies is however the use of cryogenic temperatures ( $\sim 100$  K). While allowing the more efficient electron-nucleus polarization transfer, such low temperature also leads to significant line broadenings in the NMR spectra.<sup>9,10</sup> Yet, important information can be still be extracted.

An important aspect of successful DNP experiments resides in the sample preparation, since the radicals needed to transfer polarization to the nuclei also result in paramagnetic relaxation enhancement, potentially leading to further line broadening<sup>8</sup>. Additionally, the glass-forming media often used for MAS-DNP (e.g. around 60 % of d8-glycerol) lead to reduced absolute signal due to dilution of the sample. Sedimented samples<sup>11,12</sup> have however been found to behave similarly to a glass-like environment allowing sizeable enhancements in DNP experiments even in the absence of an additional glass former like glycerol.<sup>13,14</sup>

We use the DnaB helicase from *Helicobacter pylori* (*Hp*)<sup>15</sup> as a prototypical and illustrative example to evaluate the efficiency of DNP in the characterization of protein-nucleotide interaction. Helicases are motor proteins of the replisome that unwind double-stranded DNA into their single-stranded counterparts during DNA replication.<sup>16,17</sup> Crucial for the functional understanding of DnaB helicases in the DNA replication process is to gain structural insight into ATP (as the fuel) and DNA binding to such proteins which is only partially established so

far (for a crystal structure of a bacterial helicase-DNA complex see reference<sup>18</sup>). Additionally, the mechanisms of protein-DNA interactions in DNA translocation processes is still unclear.

Here, we apply DNP-enhanced solid-state NMR to *HpDnaB* for which spectroscopy of the complex with the ATP-analogue Adenylyl-imidodisphosphate (AMP-PNP)<sup>19</sup>, as well as with ssDNA (using a polythymine oligonucleotide consisting of 20 nucleotides, (dT)<sub>20</sub>), has recently been described.<sup>20,21</sup> We find that the highest sensitivity is observed for the directly sedimented sample in the absence of glycerol. We observe an enhancement  $\epsilon$  of ca. 20 and an enhancement of roughly 6 compared to a separate experiment on a 500 MHz high-resolution solid-state NMR spectrometer in a 3.2 mm probe for the <sup>13</sup>C spins in a <sup>13</sup>C,<sup>1</sup>H cross-polarization (CP) transfer experiment with the same number of transients taking differences in magnetic field strength and spin-relaxation times into account. Sparse DNP-enhanced 2D <sup>13</sup>C,<sup>13</sup>C MAS correlation spectra only highlighting amino-acid residues involved in nucleotide binding are obtained by using an initial <sup>31</sup>P,<sup>13</sup>C polarization transfer selecting only those <sup>13</sup>C spins of the protein in the vicinity of bound nucleotides.

## Results and Discussion

### *Signal-enhancement for different sample preparations*

Figure 1 shows carbon-detected DNP enhanced CP-MAS spectra (acquired at a proton resonance frequency of 600 MHz, an electron resonance frequency of 395 GHz and at a temperature of 100 K) observed for three sample preparation protocols for *HpDnaB* reacted with AMP-PNP and ssDNA, (dT)<sub>20</sub>. The samples for DNP were prepared by *ex-situ* sedimentation at 210'000 g in a ZrO<sub>2</sub> rotor leading to a sedimented sample in the MAS rotor with a protein concentration in the order of 400 mg/mL.<sup>11,21</sup> The nitroxide biradical AMUpol was used because of the high solubility in the aqueous buffer solutions and the large DNP enhancements observed at high magnetic field strengths<sup>22</sup>. A radical concentration of 2 mM was used as a compromise between obtaining optimal DNP enhancements and preventing additional paramagnetic line broadening. Three DNP sample preparation techniques were studied for optimizing the conditions for highest sensitivity in MAS-DNP experiments. The first sample (i) was prepared using the typical buffer conditions used for DNP consisting of 60 % (v/v) d8-glycerol, 32 % (v/v) D<sub>2</sub>O and 8 % (v/v) H<sub>2</sub>O. The reactions of the protein with *HpDnaB* and AMP-PNP as well as ssDNA (for more details see Supplemental Materials Section) were performed in this buffer solution.

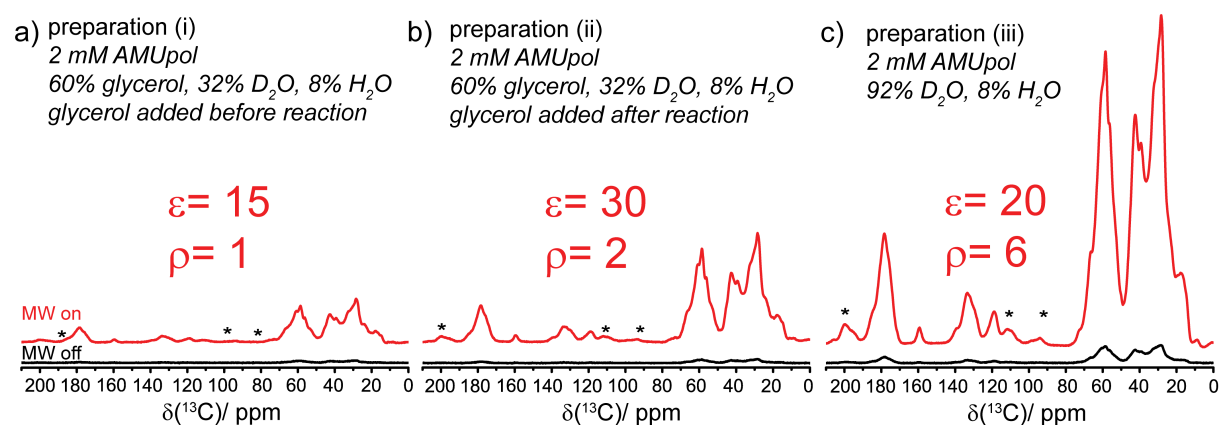


**Figure 1:** *Highest sensitivity is observed for a sedimented sample in the absence of glycerol.* Comparison of different DNP sample preparations for a *HpDnaB*:AMP-PNP:ssDNA complex, a) the complex formation was performed in a glycerol-containing buffer solution, b) glycerol was added after the complex formation, but before sedimentation, and c) no glycerol was used. In all cases the concentration of biradical AMUpol was constant at 2 mM. Enhancement factors for experiments without and with microwave (MW) irradiation ( $\epsilon$ ) and enhancements between a DNP and a conventional CP-MAS NMR experiment performed at 278 K ( $\rho = \text{SNR}^{\text{DNP}} / \text{SNR}^{\text{NMR}}$ , SNRs were determined as the ratio of the for the C $\alpha$  peak

intensity around 60 ppm intensity and noise RMSD) were determined. The values were obtained from a 1D spectrum for the peak of C $\alpha$  atoms at ~60 ppm, see Experimental Section for additional information. The  $\rho$ -values take magnetic field strength differences and different T<sub>1</sub> spin relaxation times into account.

The DNP-enhanced <sup>13</sup>C,<sup>1</sup>H CP-MAS spectrum (the DNP-enhanced <sup>1</sup>H polarization is employed as starting point in all experiments described in this work) is shown in Figure 1a and an enhancement factor between the intensity with microwaves on and off of  $\epsilon=15$  was observed (note that all spectra in Figure 1 show absolute intensities and thus can be directly compared). Since the concentration of the protein sample before ultracentrifugation (for more details of sample preparation see references<sup>11,21</sup>) is complicated by the presence of glycerol, in a second sample (ii) the reaction of *HpDnaB* with AMP-PNP and ssDNA was performed in a D<sub>2</sub>O/H<sub>2</sub>O buffer, but at higher concentrations and the solution was diluted with d8-glycerol directly prior to the sedimentation into the rotor (see Experimental Section). The DNP-enhanced <sup>13</sup>C,<sup>1</sup>H CP-MAS spectrum of this sample (see Figure 1b) shows the largest enhancements observed in our studies ( $\epsilon\sim 30$ ). Since glycerol competes with the protein during the rotor-filling processes in the ultracentrifuge which should lead to decreased sensitivity in MAS-DNP experiments, we also compared with a sample obtained by direct centrifugation in the absence of glycerol recently as described by Bertini and co-workers<sup>13,14</sup>. Figure 1c shows the DNP-enhanced <sup>13</sup>C,<sup>1</sup>H CP-MAS spectrum of an *HpDnaB*:ssDNA sedimented from a buffer containing 92 % D<sub>2</sub>O and 8 % H<sub>2</sub>O in the absence of glycerol. The DNP-enhancement ( $\epsilon=20$ ) is slightly lower than for sample (ii),  $\epsilon=30$ , but the overall signal increased significantly, nearly by a factor of three. We thus conclude that for *HpDnaB* sediments, the highest sensitivity under DNP conditions was obtained by direct ultracentrifugation out of aqueous buffer in the absence of glycerol.

For comparison, not only the enhancements characterized by  $\epsilon$  but also the enhancement compared to a standard experiment performed on a 500 MHz conventional solid-state NMR spectrometer at 278 K, called  $\rho$ , was evaluated (for details the Tables S1 and S2). These values were determined on a sedimented *HpDnaB*:ssDNA sample in the absence of d8-glycerol and radical (preparation iv) and were also corrected for differences in <sup>1</sup>H T<sub>1</sub> longitudinal spin relaxation times (1 s and 8 s under conventional and DNP conditions, respectively. For more details see Table S1). A value of  $\rho=6$  was obtained for sample (iii) which is around a factor of three smaller than the corresponding  $\epsilon$ -value. This is a

consequence of the dependence of the SNR per time unit on the longitudinal spin relaxation times ( $\text{SNR} \sim T_1^{-1/2}$ ) which are significantly longer for *HpDnaB* under DNP conditions. The  $\rho$ -values thus give a more realistic view on the gain in measurement time by DNP-enhanced experiments than the typically reported  $\epsilon$ -values. One should note that these  $\rho$ -enhancement factors are only approximate numbers as they depend on the details of the two spectrometers to be compared. Also, they were determined from 1D spectra for the overlapped C $\alpha$  region and thus line broadening effects due to the cryogenic conditions as well as paramagnetic relaxation enhancements which surely broaden a single resonance more severely and lead to lower sensitivity in higher dimensionality spectra are not taken into account.

Similar studies (sample preparation iii) were then performed on an *HpDnaB* sample reacted with ATP (instead of AMP-PNP) and ssDNA leading to a complex with *HpDnaB*:ADP:ssDNA, since ATP is hydrolyzed within the rotor filling time scale. Figure 2 shows the  $^{31}\text{P}$ ,  $^1\text{H}$  and  $^{13}\text{C}$ ,  $^1\text{H}$  DNP-enhanced CP-MAS spectra performed on a sample in the absence of glycerol. DNP-enhancements  $\epsilon$  of 19 and 23, respectively, are observed (note that no further optimization of sample preparation, e.g. variation of the radical concentration, was performed).

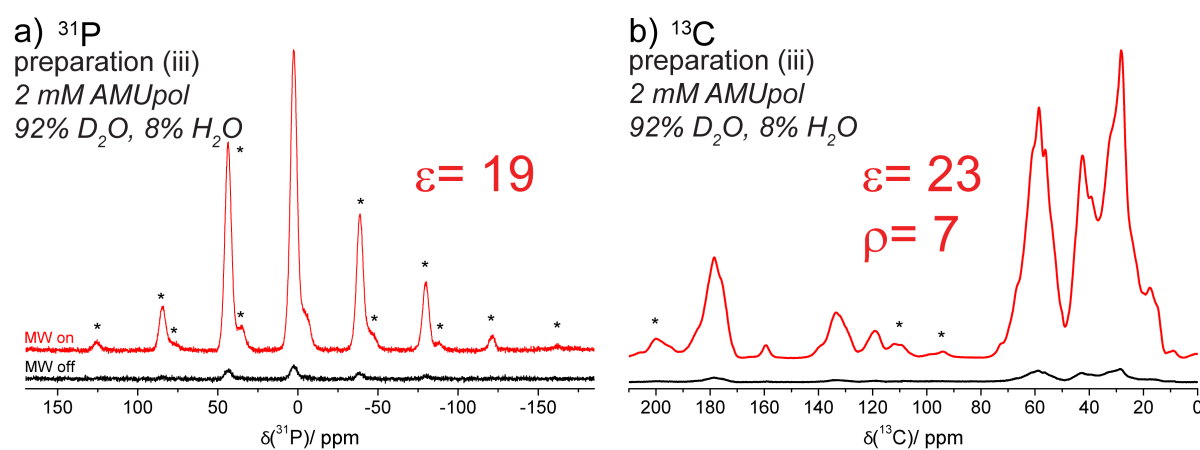


**Figure 2:** The sedimented *HpDnaB*:ADP:ssDNA complex in the presence of 2mM AMUPOL, but in the absence of glycerol. Comparison of  $^{31}\text{P}$ ,  $^1\text{H}$  CP-MAS (a) and  $^{13}\text{C}$ ,  $^1\text{H}$  CP-MAS spectra (b) for *HpDnaB*:ADP:ssDNA (ADP instead of AMP-PNP in contrast to the spectra shown in Figure 1) acquired with and without microwave irradiation at 100 K. \* marks spinning sidebands (MAS frequency 10.0 kHz). Enhancement factors for experiments without and with MW irradiation ( $\epsilon$ ) and enhancements between a DNP and a conventional NMR



experiment performed at 278 K ( $\rho = \text{SNR}^{\text{DNP}} / \text{SNR}^{\text{NMR}}$ ) were determined. The  $\rho$ -values take magnetic field strength differences and different  $T_1$  spin relaxation times into account.

We have then employed MAS-DNP to identify contacts between the protein and the nucleotide (both ssDNA and ADP). The polarization-transfer step from  $^{31}\text{P}$  of the nucleotide to the uniformly  $^{13}\text{C}$ ,  $^{15}\text{N}$  labelled protein was performed in two ways: (i) via a direct  $^{31}\text{P}$ - $^{13}\text{C}$  cross-polarization step and with (ii) a PHHC mixing step<sup>4</sup> (the pulse sequences applied are shown in Figure 3).

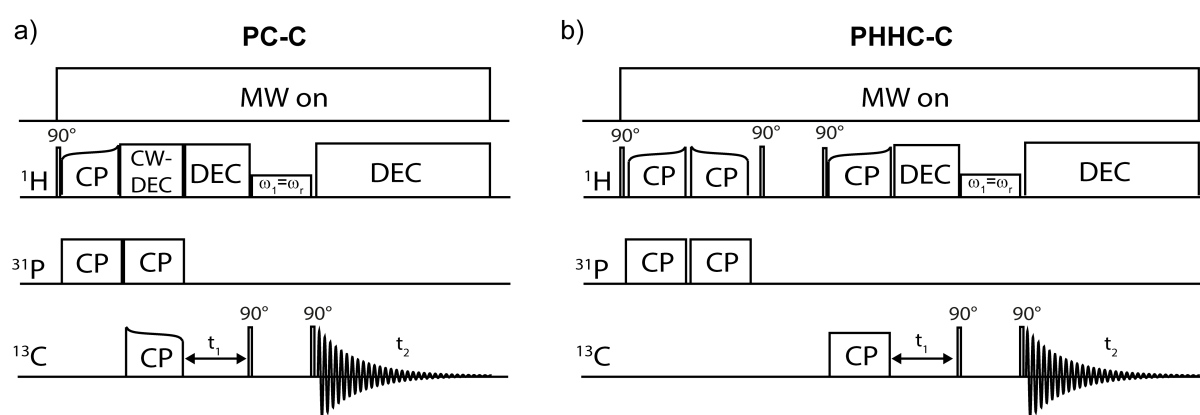


**Figure 3:** Schematic representation of DNP-enhanced a) PC-C and b) PHHC-C pulse sequence used within this work.

We note that the optimization of a direct CP step for the protein sample as used in (i) is straightforward with DNP-enhancements, but not easily achievable under conventional NMR conditions in terms of signal-to-noise ratios. To further reduce spectral overlap and to identify spin systems of residues involved in nucleotide binding, in both cases a two-dimensional  $^{13}\text{C}$ - $^{13}\text{C}$  detection step is added using 20 ms DARR mixing.<sup>23,24</sup> The corresponding spectra are shown in Figure 4 and have been recorded in 42 and 21 hours, respectively.

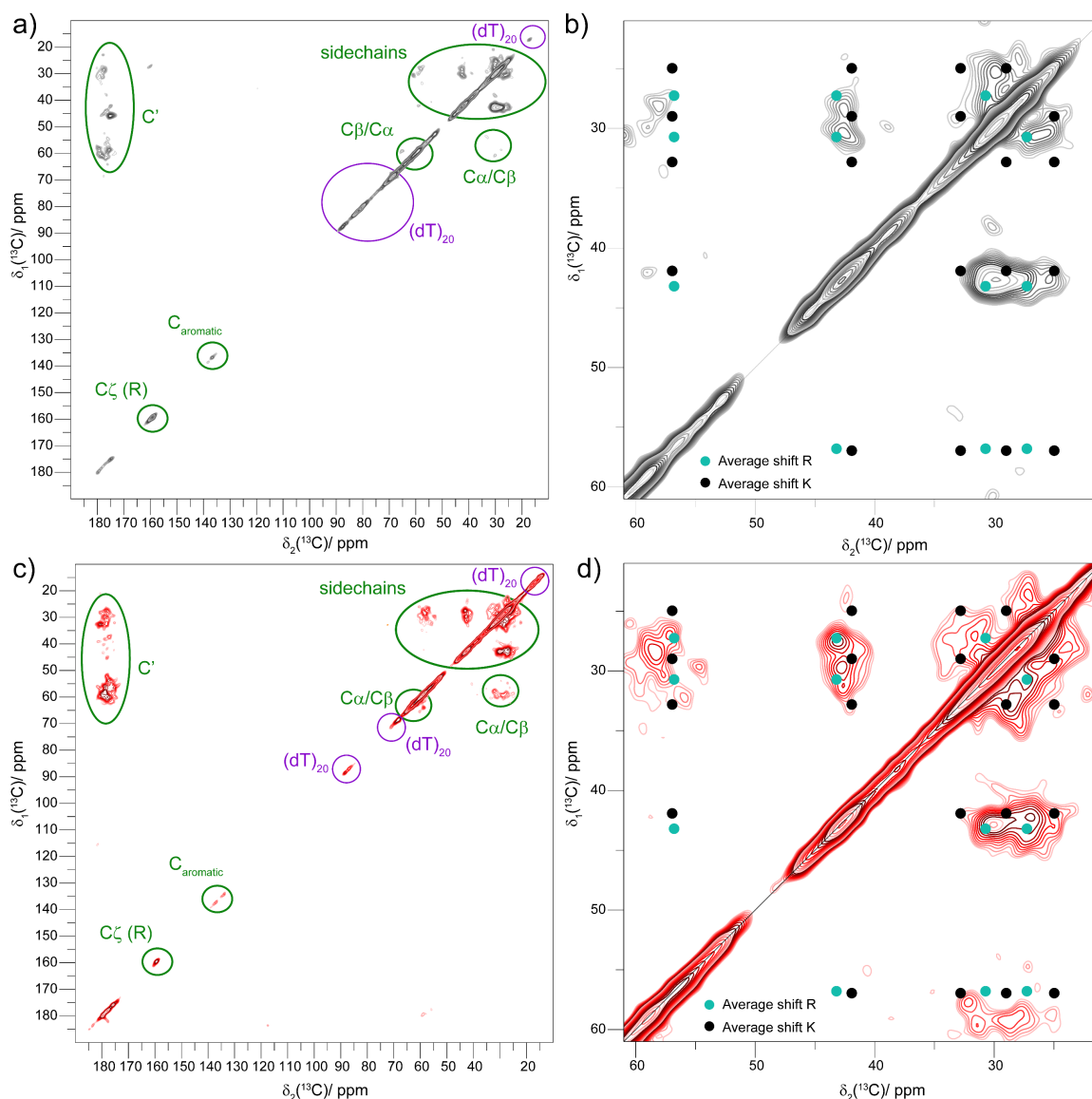


**Figure 4:** Residues in the spatial vicinity of nucleotides are detected in DNP-enhanced solid-state NMR spectra.  $^{13}\text{C}$ - $^{13}\text{C}$  correlation spectra (with 20 ms DARR mixing) of the *HpDnaB*:ADP:ssDNA complex using different  $^{31}\text{P}$ ,  $^{13}\text{C}$  magnetization transfer schemes: a) direct  $^{31}\text{P}$ - $^{13}\text{C}$  cross-polarization step with a contact time of 9 ms, and c) PHHC step with a proton-proton spin diffusion time of 500  $\mu\text{s}$ . The spectrum in a) was measured in 42 h, the spectrum in c) in 21 h. The lowest contour level in a) is at 2.6 times noise RMSD, the lowest contour level in c) at 2.1 times noise RMSD. The contour level increment is 1.1. Tentative assignments of residue types are given in the spectra. In b) and d) zooms into the aliphatic region of the spectra in a) and c) are shown, as well as the predicted peaks for arginine and lysine spin systems based on  $\text{C}\alpha$  and side-chain average chemical-shift values obtained from the BMRB database taking all proteins documented therein into account<sup>25</sup>.

The 2D PC-C spectrum in Figure 4a reveals correlations between the nucleotides and the protein (marked by green ellipsoids). Additionally, correlations between the  $^{31}\text{P}$  spins of the phosphate groups of ssDNA and  $^{13}\text{C}$  spins of the sugar and thymine base are visible on the diagonal of the spectrum (marked in purple, only on the diagonal since the ssDNA is used in natural abundance).

Characteristic spectral fingerprints for lysine and arginine spin systems are detected (for the predicted peaks based on the average chemical-shift values of lysine and arginine residues see Figure 4b and d). The spectra are asymmetric with respect to the diagonal (very dominant for correlations to the C' resonances), corroborating that the magnetization is initially transferred from the nucleotides to the sidechains spins that bind to the phosphate groups of ADP and ssDNA via hydrogen bonds. The correlations seen in the  $^{13}\text{C}$ - $^{13}\text{C}$  2D spectrum originate from the primarily intra-residue polarization transfer proceeding via DARR spin diffusion. The observed correlations to arginine sidechains (e.g. also to C $\zeta$  at around 160 ppm) agree with their role in ssDNA binding<sup>18</sup>. Further correlations to resonances of the protein are detected which are mainly involved in binding via the -OH group (e.g. serine and threonine residues) or -NH backbone via hydrogen bonds to the phosphate backbone of the nucleotides. Resonances of aromatic carbon atoms at around 135 ppm are visible as well, possibly originating from a histidine involved in nucleotide binding. Figure 5a shows a schematic representation of *HpDnaB* residues potentially involved in ADP-binding. Possible binding modes of arginine and lysine sidechains<sup>26,27</sup> to the phosphate backbone of ssDNA are given in Figure 5 b and c. While our studies clearly allow to identify spin system types in the vicinity of the nucleotides, a site-specific resonance assignment (e.g. the assignment of the observed lysine and arginine resonances to one or more of the 23 lysine and 20 arginine residues per DnaB monomer in the C-terminal domain) is precluded by the significant line-broadening at cryogenic temperatures and would in particular require additionally specific protein labeling strategies.

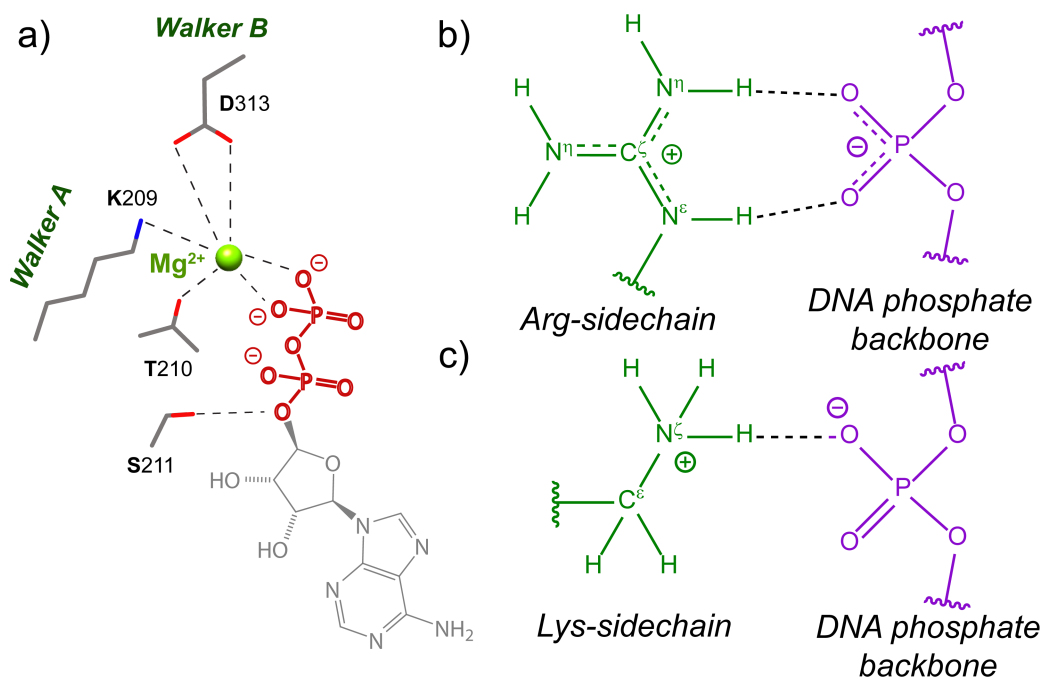


**Figure 5:** Schematic representation of the possible binding of ADP to the nucleotide-binding domain of *HpDnaB* (a) involving the Walker A and B motifs<sup>28</sup>, as well as potential binding modes<sup>26,27</sup> of arginine and lysine sidechains to the phosphate backbone of DNA (b and c). Additionally, both sidechains can potentially also coordinate to the base of DNA.

A discrimination between signals originating from ADP and ssDNA binding would in principle be possible by exploiting the different  $^{31}P$  resonance frequencies using a selective CP step<sup>29</sup> or in a 3D experiment. However, the unresolved  $^{31}P$  dimension at cryogenic temperatures made such studies impossible.

More efficient in terms of sensitivity is the MAS-DNP enhanced PHHC-C experiment (see Figure 4c) in which in general correlations to the  $C\alpha/C\beta$  are more intense. The PHHC-C spectrum has been recorded in half the measurement time compared to the PC-C experiment and is less selective than the direct  $^{31}P$ - $^{13}C$  CP polarization transfer due to the proton spin-diffusion step involved.

## Conclusions

We have demonstrated MAS-DNP-enhanced solid-state NMR detection of protein-DNA interactions in molecular motor proteins. The obtained spectra allow identification of spin system types involved in nucleotide binding, despite the typical line-broadening at cryogenic temperatures which is less of an issue in this case due to the sparsity of the spectrum.  $^{31}P$ - $^{13}C$

correlations to lysine residues, arginine sidechains and serine/threonine atoms indicate the immediate neighborhood of these residues/atoms to the  $^{31}\text{P}$  atoms of the nucleotide.

DNP enhancement factors in the order of  $\epsilon=20$  were obtained on a sedimented sample of the large oligomeric assembly of *HpDnaB* complexed with ADP and ssDNA allowing to record 2D correlation spectra in less than 24 hours. An enhancement factor of  $\rho\sim 7$  was obtained by comparing with the NMR spectra obtained at room temperature on a lower field instrument, taking into account differences in magnetic field strength and spin-lattice relaxation times. The highest sensitivity gain was observed for a sedimented sample in the absence of glycerol. Considering the linewidth issues discussed above, reduction in measurement time less than the factor of  $\rho^2\sim 50$  is practically achieved in multidimensional spectra. Nevertheless, the sensitivity gain is such that only under DNP conditions these 2D correlation spectra, including two carbon-13 dimensions, could be easily recorded.

## Experimental Section

### *Sample preparation*

AMP-PNP and ATP were purchased from Sigma-Aldrich and (dT)<sub>20</sub> from Microsynth. <sup>13</sup>C-<sup>15</sup>N labelled *HpDnaB* was prepared in buffer A (2.5 mM sodium phosphate, pH 7.5, 130 mM NaCl) as described in reference<sup>11</sup>. Three samples were prepared for DNP: (i) 0.3 mM *HpDnaB* in buffer A consisting of 60 % d8-glycerol, 32 % D<sub>2</sub>O and 8 % H<sub>2</sub>O (volume percentages are given) was mixed with 5 mM MgCl<sub>2</sub> \* 6H<sub>2</sub>O and consecutively 5 mM AMP-PNP (~18-fold molar excess of nucleotide compared to an *HpDnaB* monomer) and incubated for 2 h at 4°C. 0.5 mM of (dT)<sub>20</sub> was added and reacted for 30 min at r.t. with the *HpDnaB*:AMP-PNP complex to form the DNA-bound complex. For sample (ii) the reaction was performed at higher concentrations (0.7 mM *HpDnaB*, 11 mM MgCl<sub>2</sub> \* 6H<sub>2</sub>O, 11 mM MgCl<sub>2</sub> \* 6H<sub>2</sub>O and 1.1 mM of (dT)<sub>20</sub> in a 5.5 mM sodium phosphate and 285 mM NaCl buffer solution in D<sub>2</sub>O/H<sub>2</sub>O). The solution was concentrated in an amicon and d8-glycerol was added to achieve a 60 % d8-glycerol, 32 % D<sub>2</sub>O and 8 % H<sub>2</sub>O (volume percentages are given) buffer solution. Sample (iii) was prepared in the absence of glycerol in buffer A consisting of 92 % D<sub>2</sub>O and 8 % H<sub>2</sub>O. The *HpDnaB*:ADP:ssDNA sample was prepared with the protocol described above for sample (iii), except that ATP was used instead of AMP-PNP. In all cases, 2 mM AMUpol was added in the end and the protein/radical solution was sedimented in the MAS-NMR rotor (16 h at 4°C with 210'000 g acceleration). Thin-walled ZrO<sub>2</sub> rotors (with a volume of 42 μL) were used for all samples studied herein.

### *DNP-enhanced solid-state NMR*

DNP-enhanced solid-state NMR spectra were acquired at 14.1 T static magnetic field strength using a 3.2 mm triple-resonance (HXY) LT-MAS Bruker Biospin probe. The experiments were performed at 100 K (cooling with a cryogenic heat exchanger system) and the MAS frequency was set to 10.0 kHz. Microwaves were generated by a gyrotron emitting at 395 GHz with a power of 10 W. The 2D spectra were processed with the software TOPSPIN (version 3.2, Bruker Biospin) with a shifted (2.2) squared cosine apodization function and automated baseline correction in the indirect and direct dimensions. All spectra were analyzed with the software CcpNmr[6-8] and resonances were referenced to 4,4-dimethyl-4-silapentane-1-sulfonic acid (DSS) using adamantane as an external standard. For more experimental and processing details see the Supplemental Materials Section (Table S2).

## Acknowledgements

This work was supported by the Swiss National Science Foundation (Grant 200020\_159707 and 200020\_146757), the French ANR (ANR-14-CE09-0024B) and the ETH Career SEED-69 16-1. We cordially acknowledge the support of Laura Piveteau during one DNP session and Simon Widler for help with the expression of the protein.

## Literature

1. Wu, H., Finger, L.D. & Feigon, J. Structure Determination of Protein/RNA Complexes by NMR. in *Methods in Enzymology*, Vol. Volume 394 525-545 (Academic Press, 2005).
2. Carlomagno, T. Present and future of NMR for RNA-protein complexes: A perspective of integrated structural biology. *Journal of Magnetic Resonance* **241**, 126-136 (2014).
3. Dominguez, C., Schubert, M., Duss, O., Ravindranathan, S. & Allain, F.H.T. Structure determination and dynamics of protein-RNA complexes by NMR spectroscopy. *Progress in Nuclear Magnetic Resonance Spectroscopy* **58**, 1-61 (2011).
4. Morag, O., Abramov, G. & Goldbourt, A. Complete Chemical Shift Assignment of the ssDNA in the Filamentous Bacteriophage fd Reports on Its Conformation and on Its Interface with the Capsid Shell. *Journal of the American Chemical Society* **136**, 2292-2301 (2014).
5. Lange, A., Luca, S. & Baldus, M. Structural Constraints from Proton-Mediated Rare-Spin Correlation Spectroscopy in Rotating Solids†. *Journal of the American Chemical Society* **124**, 9704-9705 (2002).
6. Abragam, A. & Goldman, M. Principles of dynamic nuclear polarisation. *Reports on Progress in Physics* **41**, 395 (1978).
7. Abragam, A. *The Principles of Nuclear Magnetism*, (Clarendon Press Oxford, 1961).
8. Akbey, Ü. & Oschkinat, H. Structural biology applications of solid state MAS DNP NMR. *Journal of Magnetic Resonance* **269**, 213-224 (2016).
9. Bauer, T. et al. Line-Broadening in Low-Temperature Solid-State NMR Spectra of Fibrils. *Journal of Biomolecular NMR* **67**, 51-61 (2017).
10. Siemer, A.B. & McDermott, A.E. Solid-State NMR on a Type III Antifreeze Protein in the Presence of Ice. *Journal of the American Chemical Society* **130**, 17394-17399 (2008).
11. Gardiennet, C. et al. A Sedimented Sample of a 59 kDa Dodecameric Helicase Yields High-Resolution Solid-State NMR Spectra. *Angewandte Chemie International Edition* **51**, 7855-7858 (2012).
12. Bertini, I. et al. NMR properties of sedimented solutes. *Physical Chemistry Chemical Physics* **14**, 439-447 (2012).
13. Ravera, E. et al. Dynamic Nuclear Polarization of Sedimented Solutes. *Journal of the American Chemical Society* **135**, 1641-1644 (2013).
14. Ravera, E. et al. DNP-Enhanced MAS NMR of Bovine Serum Albumin Sediments and Solutions. *The Journal of Physical Chemistry B* **118**, 2957-2965 (2014).
15. Singleton, M.R., Dillingham, M.S. & Wigley, D.B. Structure and Mechanism of Helicases and Nucleic Acid Translocases. *Annual Review of Biochemistry* **76**, 23-50 (2007).
16. LeBowitz, J.H. & McMacken, R. The Escherichia coli dnaB replication protein is a DNA helicase. *Journal of Biological Chemistry* **261**, 4738-48 (1986).

17. Spies, M. *DNA Helicases and DNA Motor Proteins*, (Springer New York, 2012).
18. Itsathitphaisarn, O., Wing, Richard A., Eliason, William K., Wang, J. & Steitz, Thomas A. The Hexameric Helicase DnaB Adopts a Nonplanar Conformation during Translocation. *Cell* **151**, 267-277 (2012).
19. Yount, R.G., Babcock, D., Ballantyne, W. & Ojala, D. Adenylyl imidiodiphosphate, an adenosine triphosphate analog containing a P-N-P linkage. *Biochemistry* **10**, 2484-2489 (1971).
20. Bazin, A., Cherrier, M.V., Gutsche, I., Timmins, J. & Terradot, L. Structure and primase-mediated activation of a bacterial dodecameric replicative helicase. *Nucleic Acids Research* **43**, 8564-8576 (2015).
21. Wiegand, T. et al. Monitoring ssDNA Binding to the DnaB Helicase from *Helicobacter pylori* by Solid-State NMR Spectroscopy. *Angewandte Chemie International Edition* **55**, 14164-14168 (2016).
22. Sauvée, C. et al. Highly Efficient, Water-Soluble Polarizing Agents for Dynamic Nuclear Polarization at High Frequency. *Angewandte Chemie International Edition* **52**, 10858-10861 (2013).
23. Takegoshi, K., Nakamura, S. & Terao, T.  $^{13}\text{C}$ - $^1\text{H}$  dipolar-assisted rotational resonance in magic-angle spinning NMR. *Chemical Physics Letters* **344**, 631-637 (2001).
24. Takegoshi, K., Nakamura, S. & Terao, T.  $^{13}\text{C}$ - $^{13}\text{C}$  polarization transfer by resonant interference recoupling under magic-angle spinning in solid-state NMR. *Chemical Physics Letters* **307**, 295-302 (1999).
25. Ulrich, E.L. et al. BioMagResBank. *Nucleic Acids Research* **36**, D402-D408 (2008).
26. Esadze, A. et al. Changes in conformational dynamics of basic side chains upon protein-DNA association. *Nucleic Acids Research* **44**, 6961-6970 (2016).
27. Frigyes, D., Alber, F., Pongor, S. & Carloni, P. Arginine-phosphate salt bridges in protein-DNA complexes: a Car-Parrinello study. *Journal of Molecular Structure: THEOCHEM* **574**, 39-45 (2001).
28. Walker, J.E., Saraste, M., Runswick, M.J. & Gay, N.J. Distantly related sequences in the alpha- and beta-subunits of ATP synthase, myosin, kinases and other ATP-requiring enzymes and a common nucleotide binding fold. *The EMBO Journal* **1**, 945-951 (1982).
29. Baldus, M., Petkova, A.T., Herzfeld, J. & Griffin, R.G. Cross polarization in the tilted frame: assignment and spectral simplification in heteronuclear spin systems. *Molecular Physics* **95**, 1197-1207 (1998).